Cellular and Molecular Bioengineering, Vol. 2, No. 4, December 2009 (© 2009) pp. 495–503
DOI: 10.1007/s12195-009-0079-1

Parametric Analysis for Monitoring 2D Kinetics of Receptor–Ligand Binding

GANYUN SUN, YAN ZHANG, BO HUO, and MIAN LONG

National Microgravity Laboratory and Center for Biomechanics and Bioengineering, Institute of Mechanics, Chinese Academy of Sciences, Beijing 100190, P.R. China

(*Received 6 May 2009; accepted 29 July 2009; published online 11 August 2009*)

Abstract—Thermal fluctuation approach is widely used to monitor association kinetics of surface-bound receptor–ligand interactions. Various protocols such as sliding standard deviation (SD) analysis (SSA) and Page's test analysis (PTA) have been used to estimate two-dimensional (2D) kinetic rates from the time course of displacement of molecular carrier. In the current work, we compared the estimations from both SSA and modified PTA using measured data from an optical trap assay and simulated data from a random number generator. Our results indicated that both SSA and PTA were reliable in estimating 2D kinetic rates. Parametric analysis also demonstrated that such the estimations were sensitive to parameters such as sampling rate, sliding window size, and threshold. These results furthered the understandings in quantifying the biophysics of receptor–ligand interactions.

Keywords—Sliding standard deviation analysis, Page's test analysis, Kinetic rate, Receptor–ligand binding, Random number series.

INTRODUCTION

Cell adhesion mediated by surface-bound receptor–ligand interactions [or so-called two-dimensional (2D) binding] plays an important role in such biological processes as inflammatory reaction,[25] tumor metastasis,[1] arteriosclerosis,[11] and wound healing.[13] 2D association and dissociation kinetics governs the formation and rupture of molecular bond. While 2D kinetics of bond rupture has been extensively investigated,[2,6–8,10,16,19,22] only a few approaches have been developed to quantify 2D kinetics of bond formation using such the assays as biomembrane force probe (BFP)[5] and optical trap.[26]

To visualize the single molecular binding, two surfaces bearing respective receptors and ligands were manipulated to separate at a pre-set distance in thermal fluctuation measurements.[18,29] Ultra-sensitive probes are used to monitor the movement of molecular carrier in a weakly-damped energy well, where the displacement is in the order of several to several hundreds of nanometer (nm). Information of molecular interactions is then represented by the mean (or most probable) value and the variance of carrier thermal fluctuation. For example, 8 nm stepwise movement of single kinesin molecule[27] and 3–4 pN force transition between myosin and actin filament[9] were estimated using the mean of carrier thermal fluctuation. This mean value was also used to quantify bond lifetime and reverse rate of receptor–ligand interactions.[18,30] Variance-based analysis, e.g., sliding variance or sliding standard deviation (SD) analysis (SSA), is another method to identify the binding and unbinding states of the molecules and to measure the spring stiffness of single receptor–ligand pair.[20] Correlation analysis was applied to track individual binding events between two surfaces.[21] It has long been noticed that the readouts from these analyses strongly depend on the pre-set threshold, which is determined empirically.

The distribution function of two states, rather than their means or variances, is presumably more reliable to identify the states, as seen in two distribution-based analyses of Student's *t*-test[3] and Page's test.[17] Student's *t*-test analysis is insensitive to the threshold but requires a large ensemble of data. And the readouts eventually rely on the identification of start and end moments of the binding state. It worked well for the measurement of stepwise movement of a molecular motor[4] but may not be applicable to quantify the bond lifetime (or waiting time) of receptor–ligand interactions. Page's test analysis (PTA) employs a pairwise probability density function (PDF) to identify the states, which has been used to detect the iron-channel transition[14] and to monitor the transient mechanical events from noisy data signals.[17] It was also found that the PDF distribution of the unbinding state affected

Address correspondence to Mian Long, National Microgravity Laboratory and Center for Biomechanics and Bioengineering, Institute of Mechanics, Chinese Academy of Sciences, Beijing 100190, P.R. China. Electronic mail: mlong@imech.ac.cn

the distribution of the sequential binding state due to diffusion transportation.[32] Evidently, several parameters such as the sampling rate, the threshold, and the critical frequency of state transition affects the reliability of PDF calculation as well as of 2D kinetics estimation.

In the current work, PTA was modified and SSA[5] using measured data of thermal fluctuation measurements from an optical trap assay. Computer-generated random number series was also used to further compare the two analyses. Our results indicated that both analyses were reliable but favorable separately at different parameter sets.

MATERIALS AND METHODS

Proteins and Antibodies

Soluble L-selectin (sLs), purified PSGL-1 constructs, non-blocking anti-L-selectin monoclonal antibody (mAb) CA21, and anti-PSGL-1 mAb PL2, and blocking anti-L-selectin mAb DREG56 and anti-PSGL-1 mAb PL1 were described previously.[26] FITC-conjugated goat anti-mouse secondary mAbs and bovine serum albumin (BSA) were purchase from Sigma (St. Louis, MO, USA).

Protein Immobilization

The procedure of protein immobilization was described previously.[26] Briefly, 2.32- and 5.66 μm-diameter silica microbeads (Bangs, Fishers, IN, USA) were incubated overnight at 4 °C in 5, 10, 15, or 20 μg/ml of capturing mAbs CA21 and PL2, respectively, followed by nonspecific blocking in 2% BSA for 8 h. CA21- and PL2-coated microbeads were then incubated in 20 ng/ml of respective sLs and PSGL-1 constructs at 4 °C for over 12 h, and were ready for thermal fluctuation measurements within 3 days. Microbeads coated with BSA and CA21 or PL2 alone (all blocked with BSA) were used as control. Site density of surface-coupled sLs or PSGL-1, m_r or m_l, was determined using flow cytometry and immunoradiometric assay.[15,28]

Optical Trap Assay

Optical trap set-up was also described previously.[26] Briefly, each 10^3 sLs- and PSGL-1-coupled microbeads were injected into a customer-made glass sample cell. A sLs-coupled microbead was captured by a mobile trap (PALM, Zeiss, Germany) and was driven to the vicinity of a PSGL-1-coupled microbead pre-settled onto coverslip substrate. Time course of displacement, D_x, of sLs-coupled microbead was recorded at 25 frames per second (fps) (cf. Fig. 1a). All measurements were done at room temperature (24–28 °C).

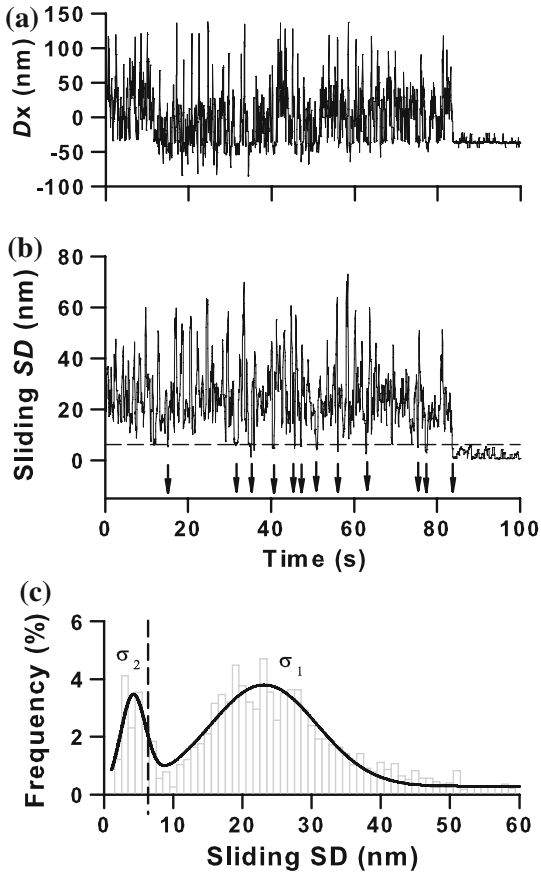

FIGURE 1. Sliding SD analysis to identify binding events from a typical displacement record monitored using an optical trap assay (a). Also plotted were the time course of corresponding sliding SD at a sliding window size of ten frames (b) and the histogram of sliding SD where two peaks represented the unbinding (σ_1) and binding (σ_2) states (c). *Dashed lines* in (b, c) were denoted as the threshold $\overline{\sigma_2} = 6.0$ nm, defined as the mean of σ_2 averaged from an ensemble of >100 records, and *arrows* indicated the binding events.

RESULTS AND DISCUSSION

SSA and PTA methods

Binding events mediated by receptor–ligand bond formation were identified by visualizing the sudden stop or sharp magnitude reduction of thermal fluctuation. A cross-correlation method described previously[12] was used to determine the position (or displacement) of sLs-coupled microbead with an accuracy of ~2 nm at focus plane. Two sets of analyses were performed to isolate the binding events from the recorded time course of displacement.

Sliding SD of displacement was calculated using a window size of ten sequential frames (Fig. 1b) and the resulted histogram was used to identify the binding state (σ_2) from the unbinding state (σ_1), as exemplified in Fig. 1c for a typical record.[5] Here the mean $\overline{\sigma_2}$, averaged from an ensemble of records ($n > 100$), was defined as the threshold (*dashed lines* in Figs. 1b and 1c) to isolate individual binding events from thermal fluctuation (Fig. 1c). Time duration underneath the threshold was the lifetime, t_r, for that event, while the interval between two sequential binding events was the waiting time, t_w. The cumulative frequency of waiting time t_w was used to predict 2D effective forward rate upon first-order irreversible reaction kinetics.[26] Two freely-adjustable parameters of the sliding window size and the threshold were required in the estimation.

PTA method, widely used to measure the statistics of PDF change for noisy signals[14,24] or to monitor the acto-myosin interactions,[17] was modified to identify the start and end moments for a binding event. The displacement for the binding and unbinding states exhibits two Gaussian histograms. For each distribution, the probability density, $f(x)$, at an arbitrary sliding SD value, x, gives,

$$f(x) = \exp\left[-(x - x_0)^2/(2\omega)\right]\Big/\sqrt{2\pi\omega}, \qquad (1)$$

where ω is the variance and x_0 is the mean value of sliding SD. The log odds ratio g is then calculated,

$$g(x) = \log_{10}\left[f_{\text{binding}}(x)/f_{\text{unbinding}}(x)\right]. \qquad (2)$$

Here g is positive if $f_{\text{binding}} > f_{\text{unbinding}}$ but negative if $f_{\text{binding}} < f_{\text{unbinding}}$. Note that high or low probability of having a positive g value is achieved when x lies in the binding or unbinding distribution, even though both positive and negative g values are found in each distribution. To determine the start and end moments of a binding event, the cumulative summation of g values, G, is calculated by assuming that negative G value denotes the unbinding state and could be discarded,[17]

$$\begin{aligned} G(0) &= 0, \\ G(t_n) &= \max\{0, G(t_{n-1}) + g(x_n)\}, \end{aligned} \qquad (3)$$

where x_n is the x value at time t_n ($n = 1, 2 \ldots N$ where N is the final data point for that series of sequential event) and $G(t_n)$ is the corresponding summation. In a forward summation, $G(t_n)$ increased with t_n since more positive g values were found in a binding distribution. Finally it reached a maximum value and then decreased sharply to zero at the end of that event (Fig. 2a), where the moment of apex was defined as the end moment for that event (*arrows* in Fig. 2a). Similarly, the start moment for that event was determined

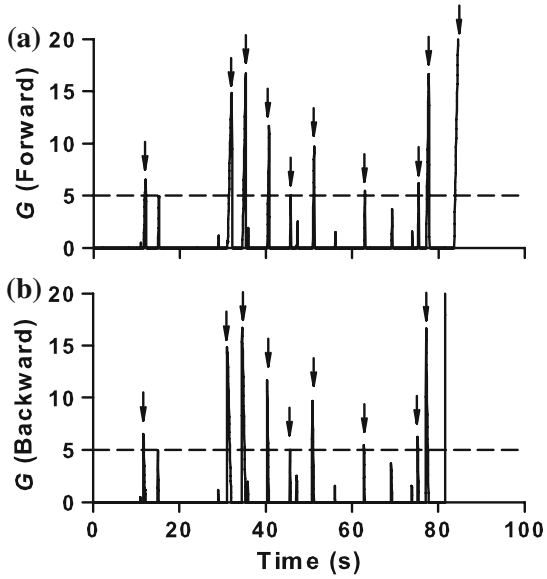

FIGURE 2. Page's test analysis to identify binding events for the typical record shown in Fig. 1. Plotted were the time courses of cumulative forward (a) and backward (b) summation *G*. *Dashed lines* in (a, b) were denoted as the threshold of 5 and *arrows* indicated the end (a) and start (b) moments for the events.

when monitoring the time course of $G(t_n)$ in a backward summation (Fig. 2b). Noting that the height of the peak so obtained is related to time duration for that event (or lifetime), the events with very short lifetimes are hard to be isolated from noise. In the current study, a threshold of 5 was applied to exclude those peaks underneath the threshold (*dashed lines* in Figs. 2a and 2b). It should be pointed out that the estimation of G value requires the distributions of $f_{\text{binding}}(x)$ and $f_{\text{unbinding}}(x)$, which depend on either both the two parameters of sliding window size and threshold (Eq. 1) or the threshold alone. Such the dependence is determined by how to define $f(x)$ at different sampling rates. At low sampling rate (as for the optical trap data), the binding and unbinding states are hard to be isolated each other using the displacement distribution, whereas the distribution of sliding SD of displacement yields two discrete peaks for the two states. Thus, $f(x)$ is defines as a function of sliding SD distribution at low sampling rate, which depends on the two parameters of sliding window size and threshold. At high sampling rate (as for those simulated data), however, the two states are able to be isolated directly from the displacement distribution and $f(x)$ can be defined as a function of displacement distribution, where only the threshold is required in PTA method at high sampling rate. Thus, less freely-adjustable parameters were employed for PTA, as compared for SSA.[17]

Identification of Start and End Moments for Binding Events

The start and end moments for a binding event was identified using the two analyses. Typically, 12 binding events were found from probability density distribution of sliding SD at a threshold of $\overline{\sigma_2} = 6.0$ nm (Fig. 1c), which started at the moment of 15.00, 31.44, 34.76, 40.32, 45.60, 47.24, 50.84, 56.06, 62.84, 75.24, 77.16, and 83.68 s, and ended at the moment of 15.16, 31.48, 35.16, 40.72, 45.76, 47.28, 51.12, 56.12, 62.96, 75.44, and 77.68 s (Fig. 1b), respectively, yielding the corresponding lifetimes of 0.16, 0.04, 0.40, 0.40, 0.16, 0.04, 0.28, 0.06, 0.12, 0.20, and 0.52 s for first 11 binding events (the 12th event was denoted as a firm adhesion event with infinite lifetime). Using the modified PTA, however, only ten binding events were unraveled at the threshold of 5, which started at the moment of 11.68, 31.04, 34.56, 40.32, 45.60, 50.84, 62.80, 75.24, 77.16, and 83.68 s, and ended at the moment of 12.16, 32.00, 35.28, 40.72, 45.76, 51.20, 62.96, 75.44, and 77.72 s with the lifetimes of 0.48, 0.96, 0.72, 0.40, 0.16, 0.36, 0.16, 0.20, 0.56 s for first nine events (Fig. 2), implying that two of those binding events observed in SSA method was not visualized in PTA method. It was also found that several start moments appeared earlier in PTA method as compared in SSA method, even for the same events.

One possibility for overestimating the number of binding events from SSA is that the readouts are much sensitive to the threshold, since less binding events would be observed when a relatively low threshold, say 5.0 nm, is set (cf. Fig. 1c). Another possibility is that such the overestimation is attributed to the statistical difference in various records from the same microbead pair and/or in different records from different pairs. To test the possibilities, an ensemble of records ($n > 100$) from >10 pairs of microbeads was pooled together to compare the readouts from two analyses. At a typical site density of $m_r \times m_l = 10.58 \times 10^5\ \mu m^{-4}$, more binding events (especially for those after first event) were identified (7001 and 994 events) with shorter lifetimes (0.32 ± 0.01 and 0.87 ± 0.03 s) from SSA than those from PTA (Table 1), suggesting that using a SSA method is able to monitor the weaker binding events but the readout is sensitive to the threshold at low sampling rate (seen as below).

Comparison of 2D Effective Forward Rate Estimation

Two-dimensional effective forward rate, $A_c k_f$, was estimated from the waiting time series using first-order irreversible reaction kinetics.[5,26] Four independent measurements at $m_r \times m_l$ = (6.54, 7.83, 9.02, 10.58) $\times 10^5\ \mu m^{-4}$ described previously[26] were employed using two analyses. $A_c k_f$ so obtained were similar [(9.3 and 9.0) $\times 10^{-8}\ \mu m^4/s$ from SSA and PTA, respectively) (Fig. 3), indicating that both the estimations were reliable. It was also found that the correlation coefficient and 2D cellular forward rate $A_c m_r m_l k_f$ were relatively higher from SSA ($R^2 = 0.96$; 0.061, 0.068, 0.085, and 0.101 s^{-1}; *squares* in Fig. 3) than those from PTA ($R^2 = 0.82$; 0.057, 0.059, 0.070, and 0.101 s^{-1}; *circles* in Fig. 3).

TABLE 1. Comparison of 2D kinetics obtained from optical trap measurements.

	SSA	PTA
Total first binding events†	46	42
Total binding events†	7001	994
Averaged lifetime (s) (mean ± SE)†	0.32 ± 0.01	0.87 ± 0.03
2D effective forward rate $A_c k_f$ ($\times 10^{-8}\ \mu m^4/s$)‡	9.3	9.0

†Data set at a site density of $10.58 \times 10^5\ \mu m^{-4}$ in Fig. 3.
‡Data sets at four different site densities in Fig. 3.

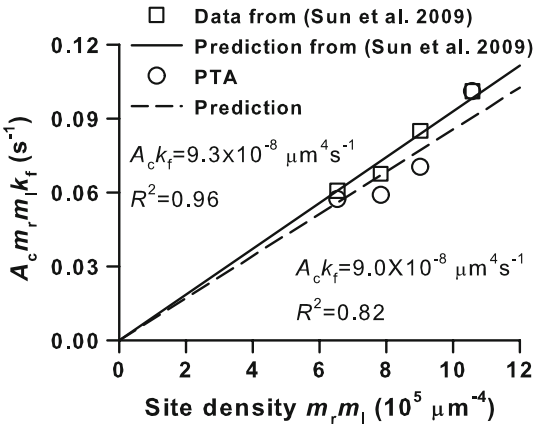

FIGURE 3. 2D cellular forward rate $A_c m_r m_l k_f$ for sLs–PSGL-1 interactions at the site densities of $m_r \times m_l$ = (6.54, 7.83, 9.02, and 10.58) $\times 10^5\ \mu m^{-4}$. Data were estimated from sliding SD (*squares*)[26] and Page's test (*circles*) analyses. *Solid*[26] and *dashed lines* were the predictions using first-order irreversible reaction kinetics. The slope of fitted line was defined as 2D effective forward rate $A_c k_f$.

Computer Simulation of Random Number Series

To further compare the readouts from two analyses, a numerical simulation was done by reproducing state-transition events where the displacement of a microbead in a weakly-damped energy well was set to follow a Gaussian distribution in temporal domain and a power spectrum density (PSD) distribution in frequency domain. Here a random number series was

produced by the random number generator, which obeys the function of PSD, PSD(f), at a frequency, f,[23]

$$\mathrm{PSD}(f) = k_B T / \left[\pi^2 \cdot 6\pi\eta r / \left(f_c^2 + f^2\right)\right] \quad (4)$$

Here f_c is the critical frequency of thermal fluctuation, k_B is the Boltzmann constant, T is the absolute temperature, η is the medium viscosity, and r is the radius of microbead. Note that $f_c = k/(2\pi \times 6\pi\eta r)$ where k is trap stiffness of force transducer (optical trap or BFP). Given a stationary Gaussian random process $Z(t)$ with zero mean, a finite random number series, $Z_i(\Delta t)$ $(1 \le i \le n)$, at a pre-set time interval Δt (the reciprocal of sampling rate) was obtained by generating an independent random number series y_1, $y_2 \ldots y_n$, which satisfies a Gaussian distribution $N(0,1)$ and iterates using the following equations,[31]

$$\begin{aligned} Z_1 &= \sigma \cdot y_1, \\ Z_i &= e^{-\alpha \cdot \Delta t} Z_{i-1} + \sigma \cdot y_i \cdot \sqrt{1 - e^{-2\alpha \cdot \Delta t}}, \quad 2 \le i \le n, \end{aligned} \quad (5)$$

where $\sigma = k_B T/(6\pi\eta r\alpha)$ and $\alpha = 2\pi f_c$. Parameters of $n = 120{,}000$, $\Delta t = 0.0002$ s, $f_c = 12{,}500$ Hz, and $\sigma = 1.4$ nm for a Gaussian noise, $f_{c1} = 3$ Hz and $\sigma = 3$ nm for a binding state, and $f_{c2} = 200$ Hz and $\sigma = 11$ nm for an unbinding state were described previously[29] and used in the current work.

The iterating strategy used here was different from the one described previously, where the Gaussian series was filtered by a single pole energy-normalized Butterworth filter.[17] Using the above parameters, a Gaussian noise series (Fig. 4a) and a state-transition series (Fig. 4b) were obtained, which were in excellent agreement with those in Veigel *et al.*[29] This consistency was further validated by comparing the PSD curve for the two series. As exemplified in Fig. 4c, the PSD yielded the similar critical frequencies but exhibited a significant difference at low f between an unbinding state (*grey line*) and a state-transition (*solid line*), indicating that a binding state is readily identified at low sampling rate (<10 Hz). Thus, the iterating strategy guaranteed to generate a reasonable random number series for kinetic rates estimation.

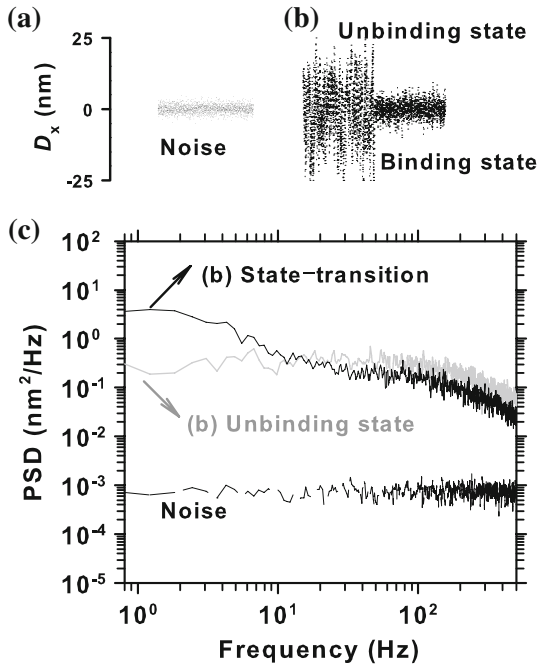

FIGURE 4. Computer-stimulated series for a Gaussian noise at f_c = 12,500 Hz and σ = 1.4 nm (a) and for a state-transition at f_{c1} = 3 Hz and σ = 3 nm (binding state) and at f_{c2} = 200 Hz and σ = 11 nm (unbinding state) (b). Also plotted were calculated PSD functions using Eq. (4) for the Gaussian noise (*dashed line*), and the state-transition (*solid line*), and the unbinding state (*grey line*) (c). Parameters of n = 120,000 and Δt = 0.0002 s described previously[29] were used.

Numerical Simulation of 2D Kinetics

The displacement magnitude and distribution in frequency domain were obtained using the above iteration (Eq. 5). The series of waiting time t_w for unbinding state and lifetime t_r for binding state were generated using pre-set kinetic parameters of forward rate k_f and reverse rate k_r, respectively. Given an arbitrary random variable x distributed uniformly in (0, 1), the series follows,[5]

$$\begin{aligned} t_w &= -\ln(1-x)/(A_c m_r m_l k_f), \\ t_r &= -\ln x / k_r. \end{aligned} \quad (6)$$

A pair of (t_w, t_r) determined the durations of two sequential unbinding and binding events. This process was repeated, which eventually reproduced a state-transition series with 120 binding events (Fig. 5a and Table 2). Here the parameters of sampling rate = 1.5×10^3 fps, σ = 1.6, and 5.3 nm for respective binding and unbinding states, $A_c m_r m_l k_f = 1.41\ \mathrm{s}^{-1}$, and $k_r = 10.16\ \mathrm{s}^{-1}$ were borrowed from Chen *et al.*[5] Given a sliding window size of 20 frames and a threshold of 2.5 nm for SSA and a threshold of 5 for PTA, more (127 events) or less (110 events) binding events were identified from the former or the latter (Figs. 5b–5d), resulting in 5.8 and 9.9% of false-negative events and 11.7 and 0% of false-positive events (Figs. 5e and 5f and Table 2). 2D kinetic rates were then estimated from two sets of t_w and t_r series from SSA and PTA, which yielded $A_c m_r m_l k_f = 1.44$ and $1.30\ \mathrm{s}^{-1}$ and $k_r = 9.94$ and $9.29\ \mathrm{s}^{-1}$ (Table 2). These results indicated that both the analyses are reliable to estimate 2D kinetic rates provided that the reasonable sliding window size and/or threshold are selected.

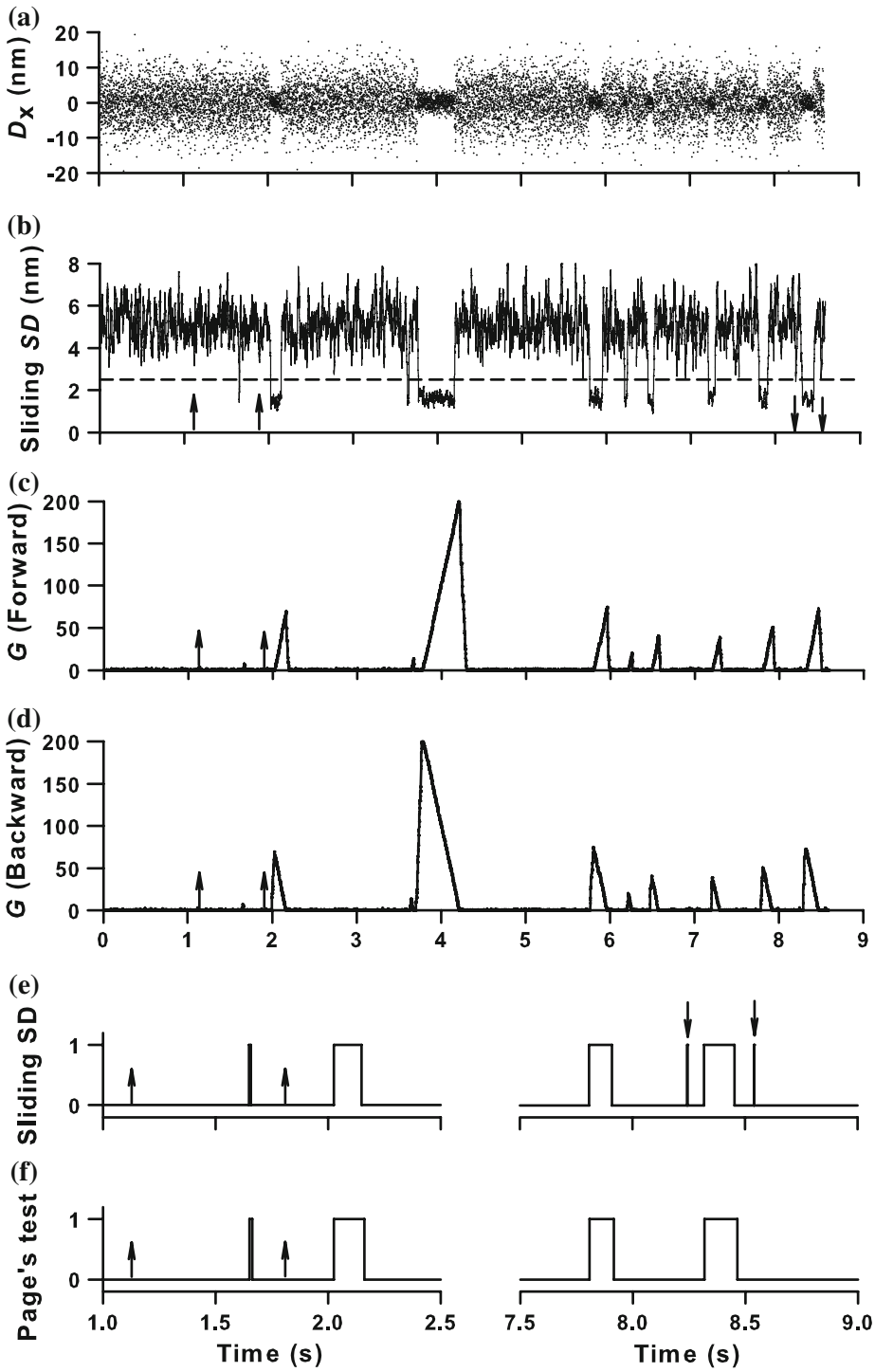

FIGURE 5. Binding event identification from a stimulated displacement record. (a) A typical series generated using the parameters in Chen *et al.*[5]: sampling rate = 1.5 × 10^3 fps, σ = 1.6, and 5.3 nm for respective binding and unbinding states, $A_c m_r m_l k_f$ = 1.41 s^{-1}, and k_r = 10.16 s^{-1}. (b) Binding event identification using sliding SD analysis at a threshold of 2.5 nm (*dashed line*) and a sliding window size of 20 frames. (c, d) Binding event identification using Page's analysis at a threshold of 5 (*lines* of the threshold are invisible) in forward (c) and backward (d) summations. (e, f) Binary plot for the segmented unbinding (set to 0) and binding (set to 1) states using the sliding SD (e) and Page's test (f) analyses. Also plotted were the false-negative (*upward arrows*) and false-positive (*downward arrows*) events (b–f).

Error Analysis of Kinetic Rate Estimation

Sampling rate, sliding window size, and threshold affect the identification of binding events and the estimation of kinetic rates. Low sampling rate underestimates 2D forward and reverse rates since those binding events with short lifetimes are potentially excluded from the entire record, which, in turn, prolongs t_w and t_r values. This is presumably why approximately tenfold higher sampling rate than critical frequency, f_c, was usually used in thermal fluctuation measurements.[23] Sampling rate also affects the kinetic rate estimation from two analyses. Here five independent data sets (100–120 data points each) were generated at five sampling rates (0.5, 1.0, 1.5, 3.0, and 6.0) $\times$ 10^3 fps. At a given threshold of 2.5 nm for SSA and 5 for PTA, the relative error, defined as the percentage of kinetic rate difference between the one from SSA or PTA and the pre-set value (cf. Table 2), increased sharply when sampling rate was reduced at $<1.0 \times 10^3$ fps (Fig. 6a). At the lowest value of 0.5×10^3 fps, the relative errors were lower in SSA method (25 and 7% for forward and reverse rates) (*open symbols*) than those in PTA method (36 and 13%) (*solid symbols*), indicating that the former might be relatively reliable at low sampling rate.

Sliding window size in SSA method may also affect kinetic rate estimation. Here six window sizes of 15, 20, 30, 40, 50, and 60 frames were used for 110 data points each set at a fixed sampling rate of 1.5×10^3 fps. It was found that the estimation was significantly affected at high (>50 frames) and low (<20 frames) window size with the high relative error of 7–47%

TABLE 2. Comparison of 2D kinetics obtained from numerical simulation.

	Pre-set value	SSA	PTA
Total events	120	127 (105.8%)	110 (91.7%)
False-negative events		7 (5.8%)	10 (9.9%)
False-positive events		14 (11.7%)	0
2D cellular forward rate, $A_c m_r m_l k_f$ (s^{-1})	1.41†	1.44	1.30
Reverse rate k_r (s^{-1})	10.16†	9.94	9.29

†Pre-set kinetic rates from Chen *et al.*[5]

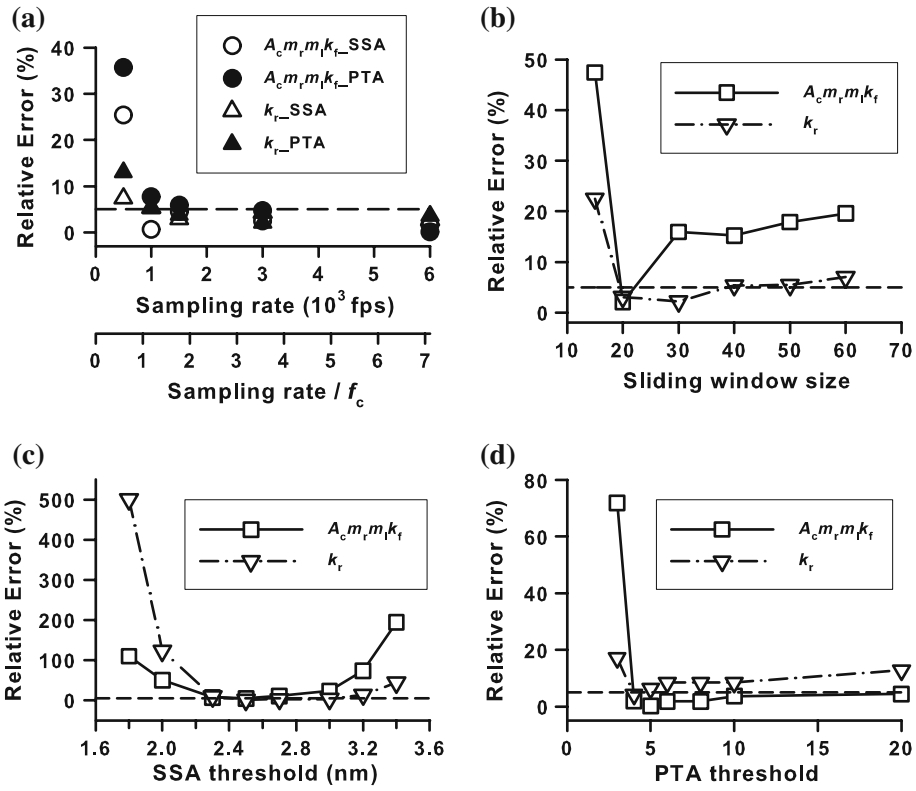

FIGURE 6. Error analysis in kinetic rate estimation. (a) Relative errors of kinetic rates difference at the varied sampling rates of (0.5, 1.0, 1.5, 3.0, and 6.0) $\times$ 10^3 fps with respective sliding window sizes of 10, 20, 20, 30, and 60 frames and at a threshold of 2.5 nm for SSA and 5 for PTA. The ratio of sampling rate to f_c (denoted as sampling rate/f_c) served as the second *x*-axis. (b) Relative errors of kinetic rates difference at the varied sliding window sizes of 15, 20, 30, 40, 50, and 60 frames for SSA, and at a fixed sampling rate of 1.5×10^3 fps and a threshold of 2.5 nm. (c) Relative errors at the varied thresholds of 1.8, 2.0, 2.3, 2.5, 2.7, 3.0, 3.2, and 3.4 nm for SSA, and at a fixed sampling rate of 3×10^3 fps and sliding window sizes of 30 frames. (d) Relative errors at the varied thresholds of 3, 4, 5, 6, 8, 10, and 20 for PTA at a fixed sampling rate of 3×10^3 fps. *Dashed line* indicated a pre-set relative error of 5%.

(Fig. 6b), indicating that SSA is sensitive to the window size used. This is because a binding event is false-negatively identified when the window size is too low or is false-positively determined when it is too high (cf. Fig. 1c), resulting in a significant difference in kinetic rate estimation. It was also indicated that the impact of window size varied with sampling rate where the critical window size (defined as the one corresponding to the lowest relative error in Fig. 6b) decreased when the sampling rate was reduced (seen below in Fig. 7a). This should not be surprised since a low sampling rate generates a small ensemble of data points and a low window size is advantageous to exclude the false-positive or false-negative events.

Threshold is another parameter to affect the estimation. Here eight thresholds of 1.8, 2.0, 2.3, 2.5, 2.7, 3.0, 3.2, and 3.4 nm, selected from $\sigma = 1.6$ nm for binding state to $\sigma = 5.3$ nm for unbinding state, were used in SSA method for 100–120 data points each set. Note that the thresholds for simulated data were lower than that for optical trap data (6.0 nm), because the distribution of sliding SD shifted leftwards at the higher spring constant for simulated data ($k \sim 10^{-1}$ pN/nm) than that for optical trap data ($k \sim 10^{-3}$ pN/nm), according to equipartition theorem $k\langle\sigma\rangle^2/2 = k_BT/2$. It was found that the estimation was significantly affected at low (<2.0 nm) and high (>3.2 nm) threshold with the high relative error of 44–500% (Fig. 6c), supporting that SSA is sensitive to the threshold used. Again, this is because a binding event is false-negatively identified when the threshold is too low or is false-positively determined when it is too high (cf. Fig 1b). The impact of threshold in PTA method, however, is different. Given seven thresholds ranging from 3 to 20 with 100–120 data points each set, the relative error increased dramatically when the threshold was reduced at <4 (Fig. 6d), presumably due to a large portion of false-positive binding events identified (cf. Fig. 2). By contrast, the relative error was retained at low level of $<10\%$ when the threshold was beyond 5, suggesting that the estimation was less sensitive to the threshold in PTA method.

Selection of Suitable Method and Parameters

The selection of the most suitable method for a set of data and the determination of optimized parameters to be used for the selected method depend mainly on the aforementioned three parameters in a thermal fluctuation assay. Another parameter is the critical frequency of thermal fluctuation, $f_c = k/(2\pi \times 6\pi\eta r)$, where k is the spring constant of force transducer (optical trap or BFP), η is the medium viscosity, and r is the radius of molecular carrier. At the given values of η and r, f_c is proportional to k. Note that not all the parameters are freely-adjustable ones; instead, they are usually correlated with each other. It is almost impossible that one method with a single set of parameters can be applied in different data sets obtained from different assays and techniques.

Here the parametric correlation was further tested. As exemplified in Fig. 7a, the dependence of critical window size on sampling rate/f_c was presented as a straight line in SSA method, implying that the window size of 20 frames be applicable for other data sets provided that the sampling rate/f_c yielded a constant of 2.0. Similar dependence was also observed in PTA method (Fig. 7b), suggesting that the threshold of 5 still works at a given ratio of sampling rate/$f_c \sim 2.0$ in different cases. Thus, the strategy to select the most suitable method and to determine the optimized parameters was proposed: (1) To choose the SSA method at sampling rate/$f_c \leq 2$ and the PTA method at sampling rate/$f_c > 2$. (2) To determine the sliding window size from Fig. 7a for SSA. (3) To define the threshold from Fig. 7b for PTA.

Finally, the sliding SD and Page's test analyses were compared to monitor 2D kinetics from measured and simulated displacement records of a carrier bearing receptors or ligands in thermal fluctuation. Similar 2D effective forward rates were obtained, imparting the confidence of two analyses in estimating 2D kinetic rates. Sliding SD analysis was found to work well at relatively low sampling rate, while Page's test analysis

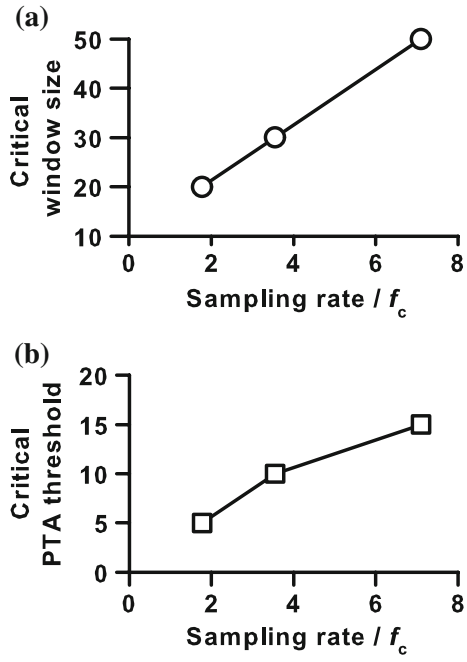

FIGURE 7. Parametric correlation for SSA and PTA. (a) Critical sliding window size increased with the ratio of sampling rate to f_c for SSA. (b) Critical threshold increased with the ratio of sampling rate to f_c for PTA.

was less sensitive to the threshold used at high sampling rate. These two analyses are also applicable for other state-transition processes.

ACKNOWLEDGMENTS

We thank Dr. R. P. McEver for generous gifts of sLs, CA21, DREG56, PL1, and PL2 proteins, and Dr. Z. Z. Ye for PSGL-1 purification. This work was supported by National Natural Science Foundation of China grants 30730032 and 30730093, National Key Basic Research Foundation of China grant 2006CB910303, National High Technology Research and Development Program of China grant 2007AA02 Z306, and Knowledge Innovation Program of CAS grant KJCX2-YW-L08.

REFERENCES

[1]Albelda, S. M. Biology of disease—role of integrins and other cell–adhesion molecules in tumor progression and metastasis. *Lab. Invest.* 68:4–17, 1993.
[2]Alon, R., D. A. Hammer, and T. A. Springer. Lifetime of the P-selectin-carbohydrate bond and its response to tensile force in hydrodynamic flow. *Nature* 374:539–542, 1995.
[3]Carter, N. J., and R. A. Cross. Mechanics of the kinesin step. *Nature* 435:308–312, 2005.
[4]Carter, B. C., M. Vershinin, and S. P. Gross. A comparison of step-detection methods: how well can you do? *Biophys. J.* 94:306–319, 2008.
[5]Chen, W., E. A. Evans, R. P. McEver, and C. Zhu. Monitoring receptor-ligand interactions between surfaces by thermal fluctuations. *Biophys. J.* 94:694–701, 2008.
[6]Chesla, S. E., P. Selvaraj, and C. Zhu. Measuring two-dimensional receptor-ligand binding kinetics by micropipette. *Biophys. J.* 75:1553–1572, 1998.
[7]Evans, E., A. Leung, D. Hammer, and S. Simon. Chemically distinct transition states govern rapid dissociation of single L-selectin bonds under force. *Proc. Natl. Acad. Sci. U.S.A.* 98:3784–3789, 2001.
[8]Evans, E., and K. Ritchie. Dynamic strength of molecular adhesion bonds. *Biophys. J.* 72:1541–1555, 1997.
[9]Finer, J. T., R. M. Simmons, and J. A. Spudich. Single myosin molecule mechanics—picoNewton forces and nanometer steps. *Nature* 368:113–119, 1994.
[10]Finger, E. B., K. D. Puri, R. Alon, M. B. Lawrence, U. H. von Andrian, and T. A. Springer. Adhesion through L-selectin requires a threshold hydrodynamic shear. *Nature* 379:266–269, 1996.
[11]Galkina, E., and K. Ley. Vascular adhesion molecules in atherosclerosis. *Arterioscl. Throm. Vasc.* 27:2292–2301, 2007.
[12]Gelles, J., B. J. Schnapp, and M. P. Sheetz. Tracking kinesin-driven movements with nanometre-scale precision. *Nature* 331:450–453, 1988.
[13]Grinnell, F. Wound repair, keratinocyte activation and integrin modulation. *J. Cell Sci.* 101:1–5, 1992.
[14]Han, C. M., P. K. Willett, and D. A. Abraham. Some methods to evaluate the performance of Page's test as used to detect transient signals. *IEEE Trans. Signal Process.* 47:2112–2127, 1999.
[15]Huang, J., J. Chen, S. E. Chesla, T. Yago, P. Mehta, R. P. McEver, C. Zhu, and M. Long. Quantifying the effects of molecular orientation and length on two-dimensional receptor-ligand binding kinetics. *J. Biol. Chem.* 279:44915–44923, 2004.
[16]Kaplanski, G., C. Farnarier, O. Tissot, A. Pierres, A. M. Benoliel, M. C. Alessi, S. Kaplanski, and P. Bongrand. Granulocyte endothelium initial adhesion—analysis of transient binding events mediated by E-selectin in a laminar shear-flow. *Biophys. J.* 64:1922–1933, 1993.
[17]Knight, A. E., C. Veigel, C. Chambers, and J. E. Molloy. Analysis of single-molecule mechanical recordings: application to acto-myosin interactions. *Prog. Biophys. Mol. Biol.* 77:45–72, 2001.
[18]Kulin, S., R. Kishore, J. B. Hubbard, and K. Helmerson. Real-time measurement of spontaneous antigen-antibody dissociation. *Biophys. J.* 83:1965–1973, 2002.
[19]Levin, J. D., H. P. Ting-Beall, and R. M. Hochmuth. Correlating the kinetics of cytokine-induced E-selectin adhesion and expression on endothelial cells. *Biophys. J.* 80:656–667, 2001.
[20]Marshall, B. T., K. K. Sarangapani, J. Wu, M. B. Lawrence, R. P. McEver, and C. Zhu. Measuring molecular elasticity by atomic force microscope cantilever fluctuations. *Biophys. J.* 90:681–692, 2006.
[21]Mehta, A. D., J. T. Finer, and J. A. Spudich. Detection of single-molecule interactions using correlated thermal diffusion. *Proc. Natl. Acad. Sci. U.S.A.* 94:7927–7931, 1997.
[22]Merkel, R., P. Nassoy, A. Leung, K. Ritchie, and E. Evans. Energy landscapes of receptor-ligand bonds explored with dynamic force spectroscopy. *Nature* 397:50–53, 1999.
[23]Neuman, K. C., and S. M. Block. Optical trapping. *Rev. Sci. Instrum.* 75:2787–2809, 2004.
[24]Page, E. S. Continuous inspection schemes. *Biometrika* 41:100–115, 1954.
[25]Springer, T. A. Traffic signals on endothelium for lymphocyte recirculation and leukocyte emigration. *Annu. Rev. Physiol.* 57:827–872, 1995.
[26]Sun, G., Y. Zhang, B. Huo, and M. Long. Surface-bound selectin-ligand binding is regulated by carrier diffusion. *Eur. Biophys. J.* 38:701–711, 2009. doi:10.1007/s00249-009-0428-y.
[27]Svoboda, K., C. F. Schmidt, B. J. Schnapp, and S. M. Block. Direct observation of kinesin stepping by optical trapping interferometry. *Nature* 365:721–727, 1993.
[28]Ushiyama, S., T. M. Laue, K. L. Moore, H. P. Erickson, and R. P. McEver. Structural and functional—characterization of monomeric soluble P-selectin and comparison with membrane P-selectin. *J. Biol. Chem.* 268:15229–15237, 1993.
[29]Veigel, C., M. L. Bartoo, D. C. White, J. C. Sparrow, and J. E. Molloy. The stiffness of rabbit skeletal actomyosin cross-bridges determined with an optical tweezers transducer. *Biophys. J.* 75:1424–1438, 1998.
[30]Veigel, C., J. E. Molloy, S. Schmitz, and J. Kendrick-Jones. Load-dependent kinetics of force production by smooth muscle myosin measured with optical tweezers. *Nat. Cell Biol.* 5:980–986, 2003.
[31]Wu, L. D., J. G. Wang, X. P. Li, and G. R. Bian. Random process. In: Probability Theory, edited by Fudan University, vol 3. Beijing: People's Education Press, 1981, pp. 374–378.
[32]Yago, T., V. I. Zarnitsyna, A. G. Klopocki, R. P. McEver, and C. Zhu. Transport governs flow-enhanced cell tethering through L-selectin at threshold shear. *Biophys. J.* 92:330–342, 2007.